High-speed Railway 1 (2023) 224–232

Contents lists available at ScienceDirect

High-speed Railway

journal homepage: www.keaipublishing.com/en/journals/high-speed-railway

Research article

Performance of the suspension method in large cross-section shallow-buried tunnels

Guoqing Cai[a,b], Xinxiang Zou[c], Qiang Zhang[d], Rui Yang[b,*], Tianchi Wu[e], Jiguang Li[f]

[a] Key Laboratory of Urban Underground Engineering of Ministry of Education, Beijing Jiaotong University, Beijing 100044, China
[b] School of Civil Engineering , Beijing Jiaotong University, Beijing 100044, China
[c] China Communications (Nanjing) Construction Co., Ltd., Nanjing 210000, China
[d] CCCC Rail Transit Technology Research and Development Center, Beijing 101304, China
[e] School of Engineering, Cardiff University, Cardiff CF24 3AA, United Kingdom
[f] Fujian Academy of Building Research Co., Ltd., Fuzhou 350025, China

ARTICLE INFO

Keywords:
Subway tunnel construction
Suspension method
Settlement control
Numerical analysis
On-site monitoring

ABSTRACT

Large cross-section tunnel construction induces ground surface settlements, potentially endangering both subterranean projects and nearby above-ground structures. A novel tunnel construction method, known as the suspension method, is introduced in this paper to mitigate surface settlement. The suspension method employs vertical tie rods to establish a structural connection between the initial tunnel support system and the surface steel beam, thereby exerting effective control settlements. To analyze the performance of the proposed method, systematic numerical simulations were conducted based on the practical engineering of Harbin Subway Line 3. The surface settlement and vault settlement characteristics during construction are investigated. The results show a gradual increment in both surface and vault settlement throughout the construction process, culminating in a stabilized state upon the completion of construction. In addition, compared to the double-side drift method and the Cross Diaphragm Method (CRD) method, the suspension method can obviously reduce the surface settlement and vault settlement. Moreover, the surface settlements and the axial force of tie rods were continuously monitored during the construction process at the trial tunnel block. These specific monitoring measurements are illustrated in comparison to numerical analysis results. The monitored results show great agreement with the numerical predictions, confirming the success of the project. This research can serve as a valuable practical reference for similar projects, offering insights and guidance for addressing ground surface settlements and enhancing construction safety in the domain of large cross-section tunneling.

1. Introduction

Railway tunnels have emerged as indispensable elements of contemporary urban infrastructure, addressing the growing transportation demands of densely populated cities. Tunnel construction techniques play a pivotal role in shaping the development of these vital transit systems [1]. However, owing to the characteristics of shallowly buried and large spans of tunneling, it usually results in a significant ground surface settlement, potentially leading to severe harm to adjacent structures and subterranean pipelines, particularly in urban areas [2–4]. The need to manage ground surface settlements in urban areas is widely acknowledged, driving the ongoing development of innovative construction techniques [5–7].

The Shallow Tunneling Method (STM) has been extensively employed [8–10] in the construction of tunnels buried shallowly in the soft ground due to its capability of reducing surface disruption and minimizing impacts on buried pipelines and other existing structures situated close to the tunneling route [11]. Sequential Excavation Methods (SEM) have been devised to partition the tunnel face into multiple temporary drifts to reduce ground displacement [12–14]. Sequential excavation can be classified into different categories according to its construction sequence, e.g., top-heading-and-bench method, Cross Diaphragm Method (CRD), both side drift method and three-bench seven-step excavation method [15]. Li et al. [16] discussed the mechanical and displacement characteristics of a shallow buried tunnel excavation by the three-bench seven-step method. Fang et al. [15] analyzed the mechanical responses of a high-speed railway tunnel excavated in shallowly buried soft ground with irregular surface topography using the CRD method. The results show that the magnitude of

* Corresponding author.
E-mail address: ruiyang1@bjtu.edu.cn (R. Yang).

https://doi.org/10.1016/j.hspr.2023.11.002
Received 5 October 2023; Received in revised form 31 October 2023; Accepted 6 November 2023
Available online 22 November 2023

ground settlement induced by tunneling varies in accordance with the geometric features of the partitioned face, including the size and distribution of the drifts [17]. Zhang et al. [18] suggested that temporary support is the key point when using SEM in most tunnel construction, because of the large deformation and complex force involved in its construction and demolition. Previous studies have made remarkable progress in controlling ground surface settlements for shallow buried tunnels. However, as urbanization advances, the geological conditions for subway construction have become more complex, requiring more stringent surface settlement control than what current methods can provide.

In this paper, a novel tunnel excavation method, namely the suspension method is proposed to control the surface settlement. Vertical tie rods are employed in the proposed method to establish a connection between the initial tunnel support structure and the surface steel beam, thereby effectively controlling settlements. Then, a comprehensive study focused on the application of the suspension method in the construction of Harbin Subway Line 3 is discussed. Furthermore, numerical results are presented to validate the performance of the proposed method. Finally, the monitoring results associated with tunnel construction, including the ground surface settlements and axial force of tie rods are reported and illustrated. This research provides valuable insights into the benefits and efficacy of the suspension method as a sustainable approach to urban tunnel construction.

2. Proposed construction method

A novel suspension method has been proposed for the construction of shallow buried underground metro tunnels, which integrates the CRD method and suspension bridge theory. The proposed method involves the construction of steel beams on the ground surface, which are then connected to the tunnel lining through prestressed tie rods. The suspension effect generated by the beams and tie rods is utilized to control and reduce the ground displacement that results from stress release after tunnel excavation. In turn, this leads to a significant improvement in construction safety and a reduction in the negative impact on the surrounding environment. The construction process of the proposed method is presented in Fig. 1.

The concrete beams and steel longitudinal beams are erected on the ground surface before tunnel excavation, with boreholes serving as a guide for drilling into the stratum (Fig. 1(a)). Then, advanced small pipes are laid for grouting to ensure the stability of the tunnel face (Fig. 1(b)). Next, the large section of the whole excavation is divided into 4 small pilots. The corresponding primary supports are installed

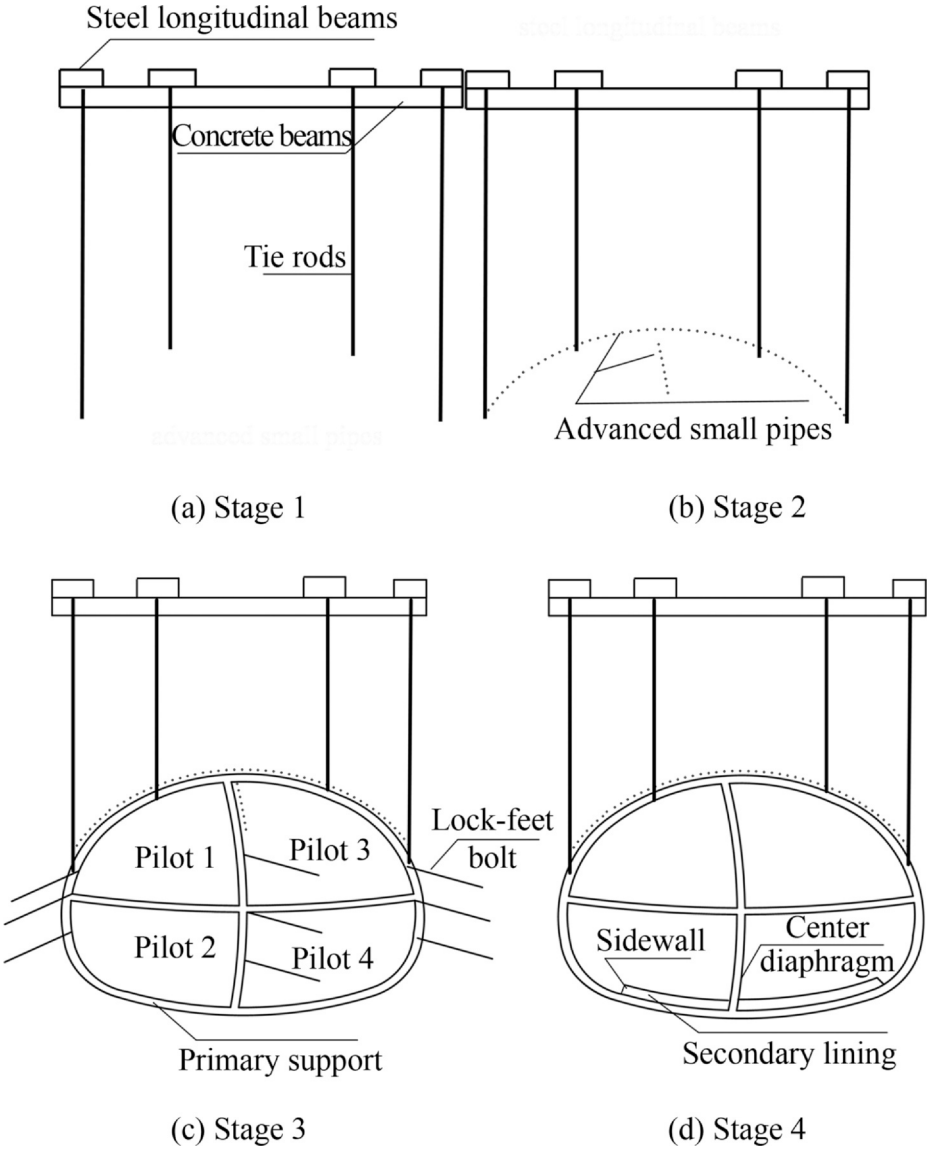

Fig. 1. Construction steps of the proposed suspension method.

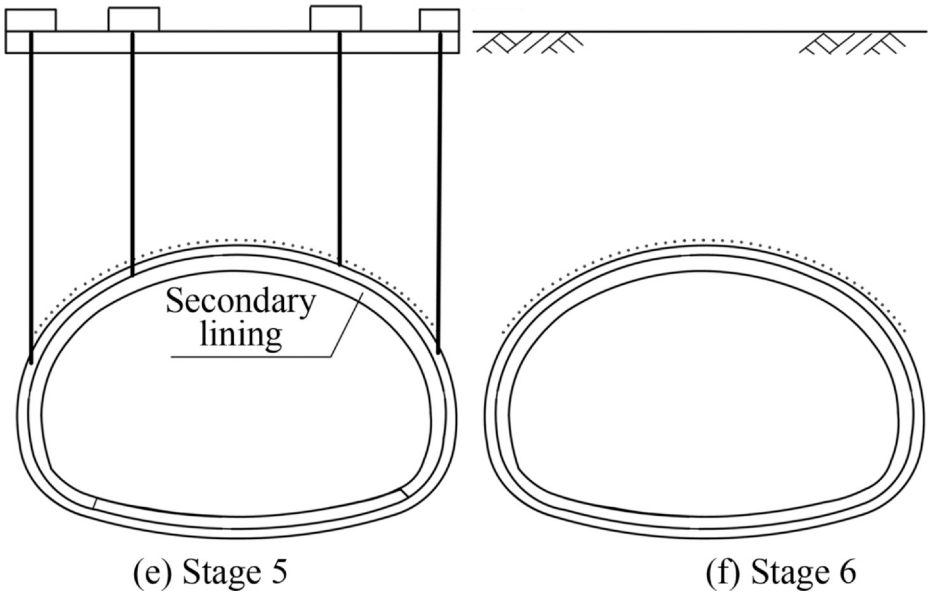

Fig. 1. (*continued*)

immediately after excavation. Bolt-mesh-spurting, grille and steel arch are selected as the primary support. At the same time, lock-feet bolts are used at the foot of each grille of all the pilots to control the deformation. Each excavation step promptly formed a complete and stable force system. Then, the tie rods are installed and prestressed through the pre-drilled boreholes on the tie beams for connecting the primary support and tie beams (Fig. 1(c)). After that, a part of the center diaphragm is removed, and the waterproofing membrane, secondary lining of the bottom plate and part of the sidewall are installed. Once the bottom arch structure reaches the design strength, the temporary center diaphragm is braced back to the bottom plate (Fig. 1(d)). The temporary inverted arch and center diaphragm are removed at regular intervals. The secondary lining of the sidewalls is carried out to form a closed ring (Fig. 1(e)). Finally, all temporary support components are dismantled after the secondary lining has achieved the required design strength (Fig. 1(f)).

3. Numerical simulations

Numerical simulations were performed to demonstrate the performance of the aforementioned construction method. Typical construction sections in practical engineering were selected as prototypes for the numerical model. The deformation and settlement of the ground during excavation were analyzed.

3.1. In-field description

The Harbin Metro Line 3 is a circular line in the rail transit network, playing a critical role in evacuating passengers and alleviating traffic congestion in the central area. A trial area for implementing the suspension method was selected along a section of Metro Line 3, from chainage K17 + 196.652 to chainage K17 + 222.409. As illustrated in Fig. 2, the trial area extends to the tunnel with a span of 12.2 m to the south and connects to the southern end of the Harbin Turbine Company Station (HTCS) to the north. The area is surrounded by dense turbine plant buildings, which contain a substantial amount of precision instruments such that surface subsidence needs to be strictly controlled during the tunnel construction period to prevent excessive deformation and potential economic losses. The enclosure construction site of HTCS offers a flat terrain that can meet the construction requirements for the installation of transverse and longitudinal beams.

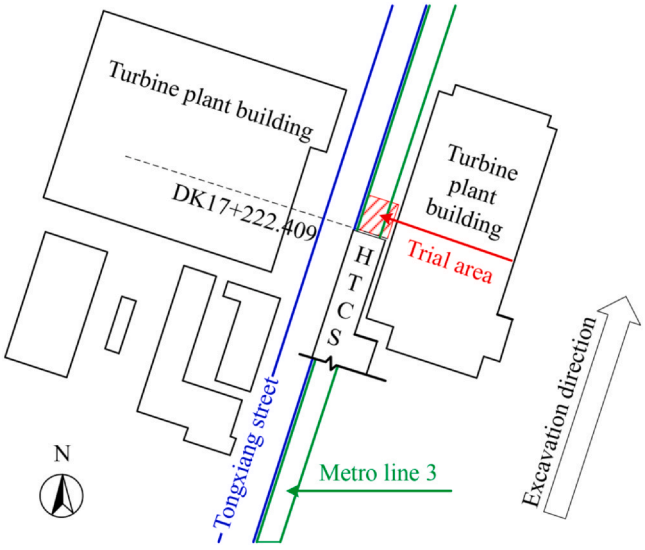

Fig. 2. Layout of the project site.

A typical transverse profile of the trial area is shown in Fig. 3. It reveals that the ground is composed of three distinct stratigraphic layers: back fill (about 3.1 m thick), silty clay (about 27.5 m thick) and sand (about 13.4 m thick). The tunnel is situated within the silty clay layer, while the groundwater is deeply buried at a depth of 11.0 m under the temporary inverted arch. The excavation width and height of the cross-section tunnel are 13.8 and 11.0 m, respectively. The average buried depth of the overlying soil on the top of the tunnel is approximately 11.06 m which is nearly equal to the excavation height. The construction of the tunnel using the suspension method commenced on September 7th 2018, and was completed on August 12nd 2019.

3.2. Numerical model

The numerical simulation in this paper was carried out using the widely-used commercial software Abaqus, which employs a pre- and post-processing finite element program commonly utilized for analyzing geotechnical problems. The numerical model, as shown in

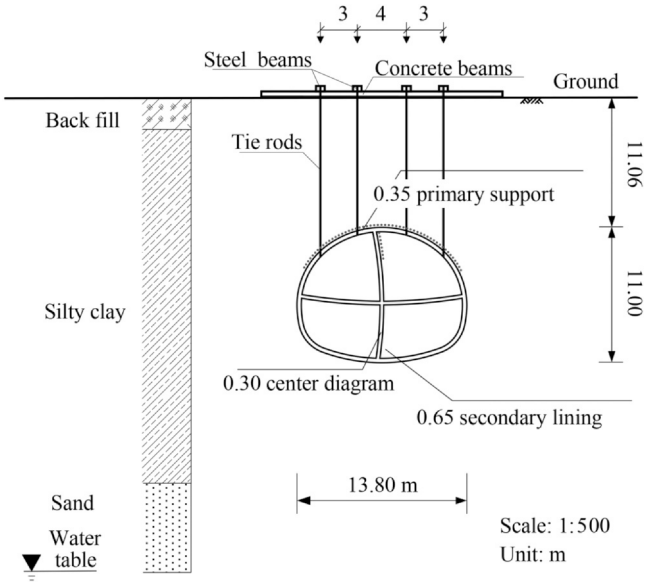

Fig. 3. The typical geological profile of the trial area.

Fig. 4(a), was established for the above-mentioned tunnel section. The model takes into account the stratigraphic layers identified in the site investigation and the supporting system employed during construction. Fig. 4(b) illustrates the supporting system of the tunnel. To reduce the influence of boundary effects on numerical results, it is imperative to ensure that the dimensions of the model exceed three times the height and diameter of the tunnel. Thus, the model dimensions in the *X*, *Y*, and *Z* directions were determined to span an expanse of 94, 56, and 44 m, respectively. The model was discretized into a total of 60584 elements and 65880 nodes. Hexahedral elements representing the surrounding soils adjacent to the tunnel were refined to accurately capture the behavior of the surrounding soils. Displacement boundary conditions were modeled by fixing vertical displacement on the bottom surface and fixing horizontal displacement on the left, right, front, and backward surfaces of the model. The surface of the model was free of constraints. The behavior of the soil was described using a linear elastic constitutive model conforming to the Drucker-Prager failure criterion. The soils, concrete beams and steel longitudinal beams conducted on the ground and lining structures (primary lining and secondary lining) were modeled using solid elements, while the tie rods were simulated using beam elements with the two ends of the tie rods being connected to the steel longitudinal beams and lining structure respective. Lock-feet bolts are represented by cable elements. Both the temporary middle wall and advanced small pipe grouting are modeled by changing soil parameters. Fig. 4(c) displays the zone of lining and temporary middle wall. The geotechnical parameters of different layers and the mechanical parameters of supporting structures for the analysis are summarized in Table 1.

The construction process was simplified into four stages for the purpose of ease of calculation: 1) excavation of pilot 1 and pilot 2, followed by the construction of primary support, which was divided into 21 steps; 2) excavation of pilot 3 and pilot 4, followed by the construction of primary support, which was divided into 13 steps; 3) removal of the center diagram, followed by the construction of secondary lining, which was divided into 5 steps; 4) removal of the tie rods and surface steel frame system, which consisted of 1 step.

3.3. Simulation results

Fig. 5 shows the ground surface settlement contour of a transverse section at different construction stages. It can be observed from Fig. 5 that as the construction progresses, the maximum surface settlement steadily increases. During the primary support stage of the excavation

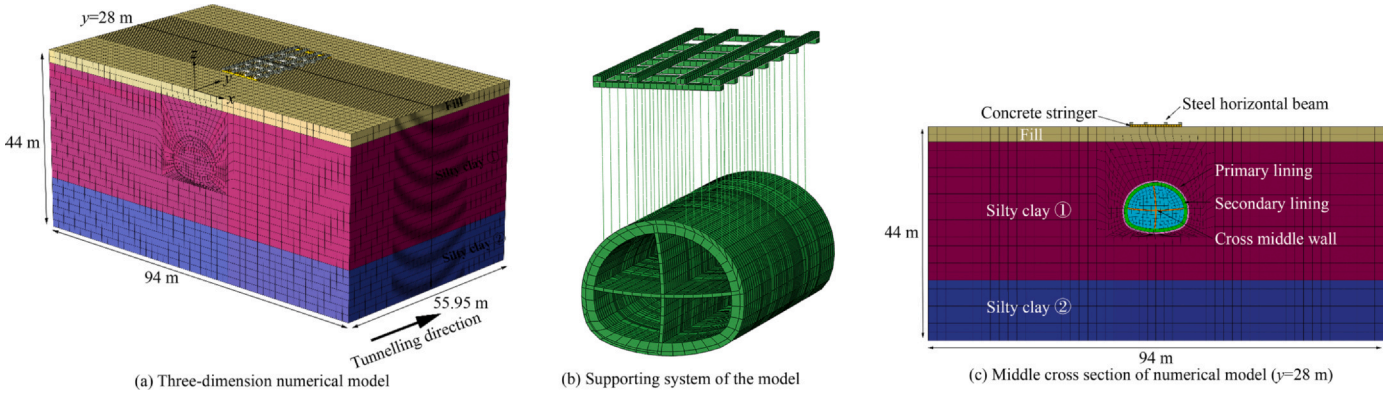

(a) Three-dimension numerical model (b) Supporting system of the model (c) Middle cross section of numerical model (*y*=28 m)

Fig. 4. Numerical model of the tunnel.

Table 1
The relevant materials parameter of the numerical model.

Material	Layer thickness/m	Elastic modulus/MPa	Poisson's ratio	Cohesion/kPa	Internal friction angle/(°)	Specific weight/kg·m^{-3}
Back fill	3.1	10	0.25	11	10	1800
Silty clay	27.5	30	0.3	26	18	1900
Sand	13.4	60	0.3	0	28	1930
Advanced grouting pipe	–	300	0.3	60	35	2150
Primary lining	–	28000	0.2	–	–	2360
Secondary lining	–	31500	0.2	–	–	2360
Concrete beam	–	30000	0.2	–	–	2360
Steel beam	–	200000	0.3	–	–	2400
Tie rod	–	200000	0.3	–	–	2400

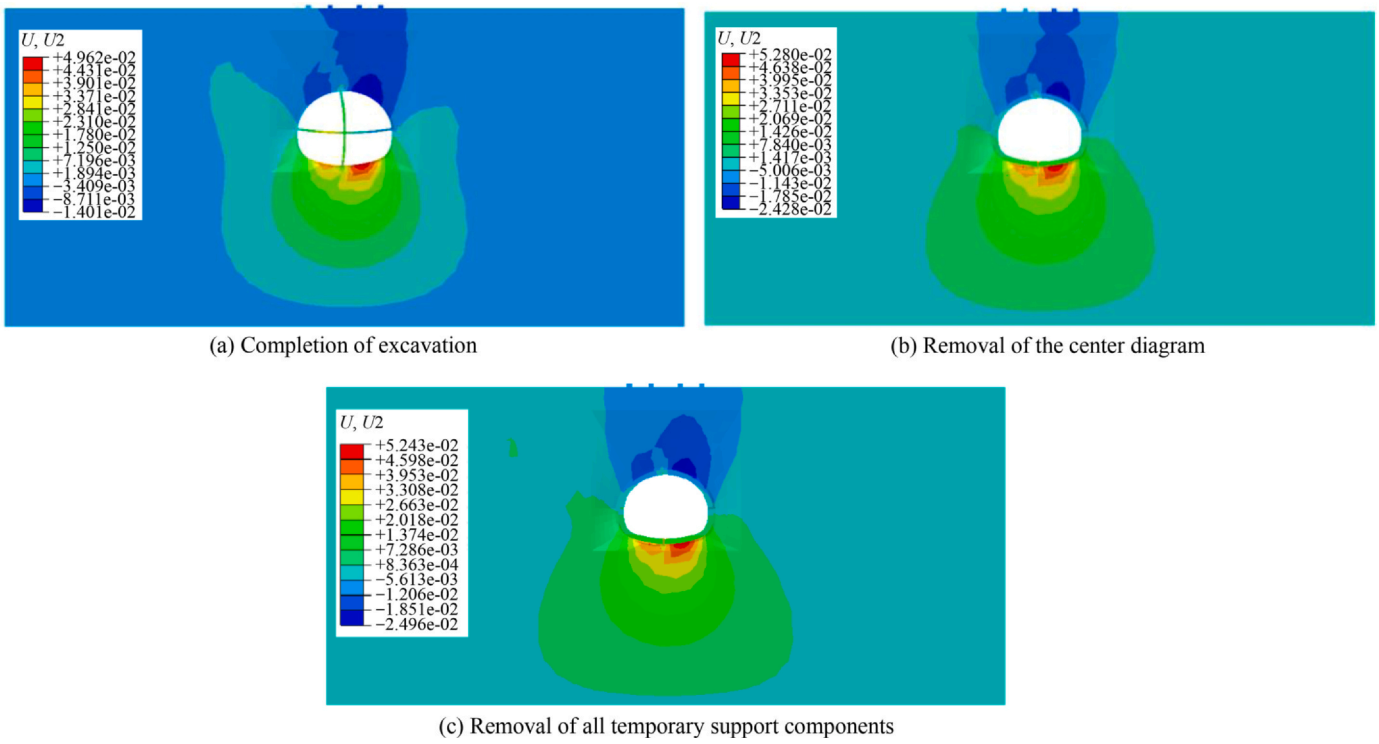

Fig. 5. Ground surface settlement contour of a transverse section at different construction stages.

and construction of the 3rd and 4th pilot tunnels (Fig. 5(a)), due to the strain alleviation in the soil layers that were excavated, the maximum surface settlement reached 6.3 mm. As the center diagram was removed (Fig. 5(b)), the lack of support from the soil caused the maximum surface settlement to further increase, reaching 12.9 mm. Following the dismantling of the tie rods and surface steel frame system (Phase 4), the tension on the soil layer was eliminated, leading to the release of additional stress, resulting in a maximum surface settlement of 14.5 mm.

To verify the effectiveness of the suspension method, the surface settlement and vault settlement generated by the suspension method are compared with those of other construction methods. To obtain a better comparison, it is assumed that these approaches are used under the same conditions. Numerical models for the above-mentioned project were established with the double-side drift method and CRD method, respectively. The simulated ground surface settlements of the study region for different construction approaches are shown in Fig. 6. It can be observed from Fig. 6 that the ground surface deformation caused by tunneling is mainly characterized by settlement, with ground heave occurring at locations far away from the tunnel centerline. The degree of settlement differs with the construction method employed, but the maximum surface settlement is consistently observed in the vicinity of the tunnel centerline. The proposed suspension method exhibits superior performance in surface settlement control compared with the double-side drift method and CRD method, with a maximum settlement of 14.51 mm.

Fig. 7 plots the simulated settlements of the vault versus the construction sequence. The vault settlement increases as the tunnel excavation progresses as illustrated in Fig. 7. With the competition of secondary lining, the simulated final vault settlements for the suspension method, the double-side drift method, and the CRD method are 24.95, 32.32, and 36.30 mm, respectively. The CRD method produces the greatest displacement of the vault among the three construction methods at all the construction stages. The double-side drift method exhibits lower initial deformation of the vault during tunnel excavation.

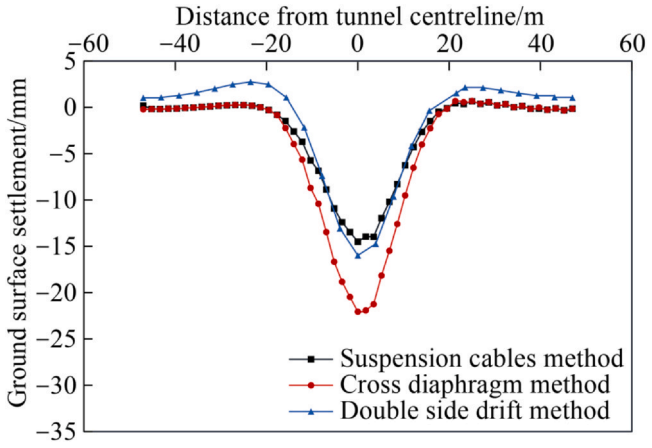

Fig. 6. Ground surface settlements for different construction methods.

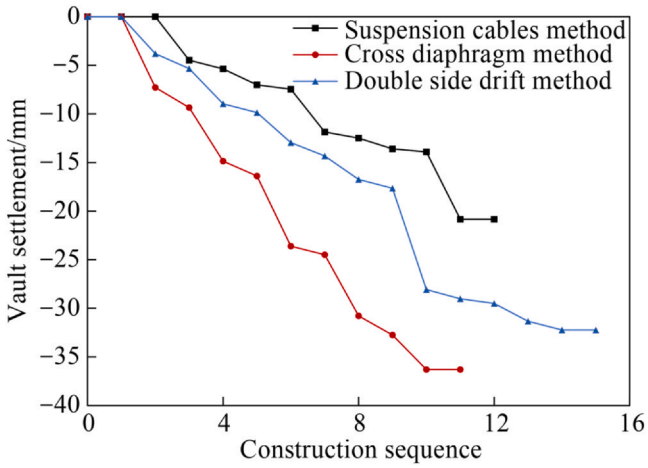

Fig. 7. Vault settlements for different construction methods.

However, as the excavation progresses to the fifth drift, the settlement increases significantly. The proposed suspension method yields the smallest settlement of the vault compared to the other methods. To ensure the safe operation of existing roads and buildings during tunnel construction, according to the technical code for monitoring measurement of subway engineering (DB11 409–2007), the surface settlement and the vault settlement of the tunnel shall not exceed 30 mm. Traditional methods are inadequate in meeting the code requirements for the vault settlement. The suspension method shows its superiority by effectively controlling surface and vault settlements by connecting the initial tunnel support structure with the surface steel frame system through vertical tie rods.

4. On site monitoring results and discussions

4.1. Layout of monitoring points

For the stability of the tunnel and the adjacent structures, a comprehensive on-site monitoring program has been systematically implemented, encompassing the settlements of ground surface settlements, and the axial force of tie rods. Monitoring program lasted 365 days from 7th September 2018 to 7th September 2019, with a daily monitoring frequency. The spatial distribution of the monitoring points within the study area is shown in Fig. 8. For the monitoring of ground surface settlements, a network of fifteen monitoring points was positioned across three distinct sections. These points were organized in a grid pattern consisting of three columns aligned with the tunneling direction and five rows perpendicular to them. Specifically, the monitoring point in row two was located directly above Pilot Drift 3, the third row aligned with the tunnel's centerline. Meanwhile, the point in the fourth row was located above Pilot Drift 1. In addition, a total of twenty-four points were installed to monitor the axial forces in the tie rods.

4.2. Ground surface settlements

The ground surface settlement measurements of specific monitored points are depicted in Fig. 9. It is evident from Fig. 9 that the ground surface experienced noticeable settlement at the tunnel excavation stage. Subsequently, tunnel construction activities were suspended due to adverse weather conditions following the completion of tunnel excavation on December 7th, 2018. During the winter construction break, the surface settlements still exhibit significant fluctuations. This is primarily attributed to the freezing of the soil in winter and subsequent thawing in spring. During the initial phase of the construction break, as temperatures drop, the ground begins to freeze which can lead to a slight uplift of the ground surface. Once the soil is fully frozen, the rate of settlement change decreases, and the surface remains relatively steady. Upon the arrival of spring and rising temperatures, the thawing process induces noticeable settlement in the ground surface. Following the thaw period, the ground surface tends to stabilize once more. The maximum settlement during winter construction is 9 mm in mid-April as shown in Fig. 9. After six six-month hiatus, the construction project resumed on June 3rd 2019. The existing tunnel supports and temporary linings were removed, and the permanent secondary lining was cast resulting in additional settlement as a result of the adjustment and casting processes. Subsequently, the surface settlement was effectively controlled after the completion of the secondary lining. Results of the final monitoring revealed that the maximum settlement of the trial area was 15.21 mm, which is far less than the allowable value, thus demonstrating the successful application of the proposed method. It can also be observed from Fig. 9 that the monitoring points situated directly above the tunnel's centerline (D1–5, D2–5 and D3–5 points) within the same column exhibited the most significant settlement. Furthermore, the settlements located above Pilot Drift 1 were commonly greater than that above Pilot Drift 3. This phenomenon arises due to increased soil and rock disturbance and loosening during the initial excavation phase, resulting in greater ground surface settlement.

Fig. 10 displays a comparison between the simulated and on-site monitoring values for ground surface settlement at monitoring points. It is evident that, upon completion of the construction, the simulated and on-site monitoring values for ground surface settlement at monitoring point D2–3 were 13.96 and 12.58 mm, respectively, while at monitoring point D2–4, the corresponding values were 14.51 and 14.89 mm. Both the monitoring results and numerical analysis show similar trends in settlement curve variations, particularly during the central partition removal phase (construction steps 35–39), where they closely align.

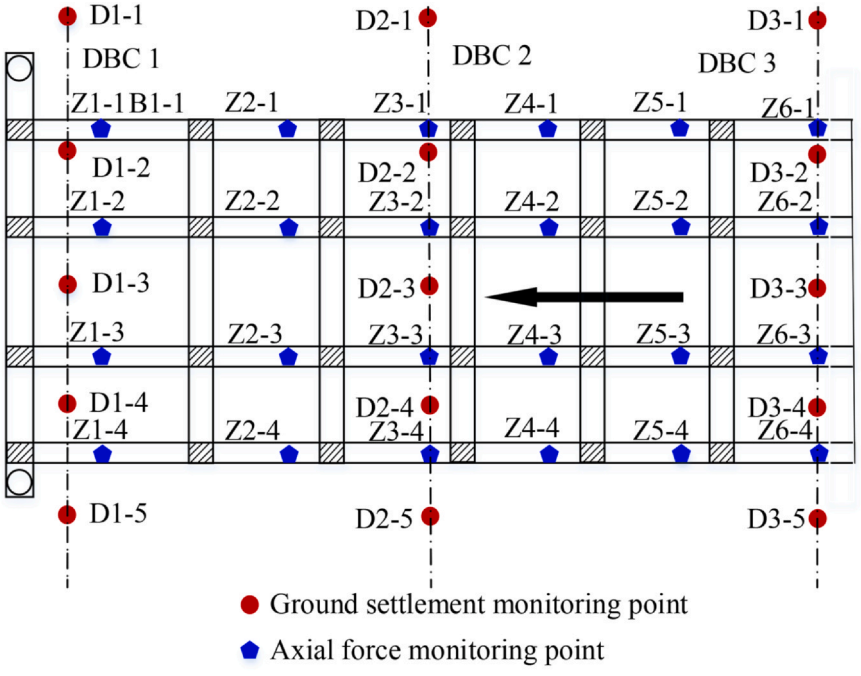

Fig. 8. Layout of monitoring points.

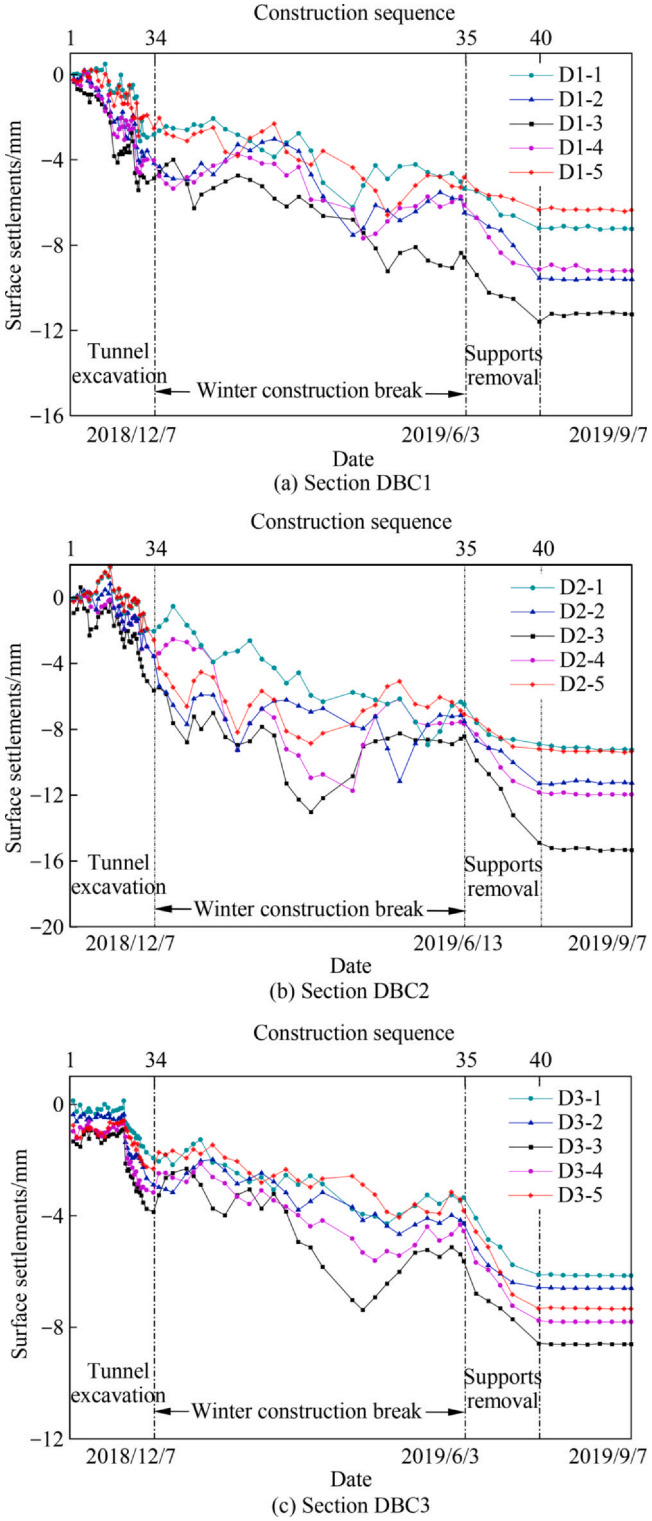

Fig. 9. Monitored ground surface settlements for the trial tunnel.

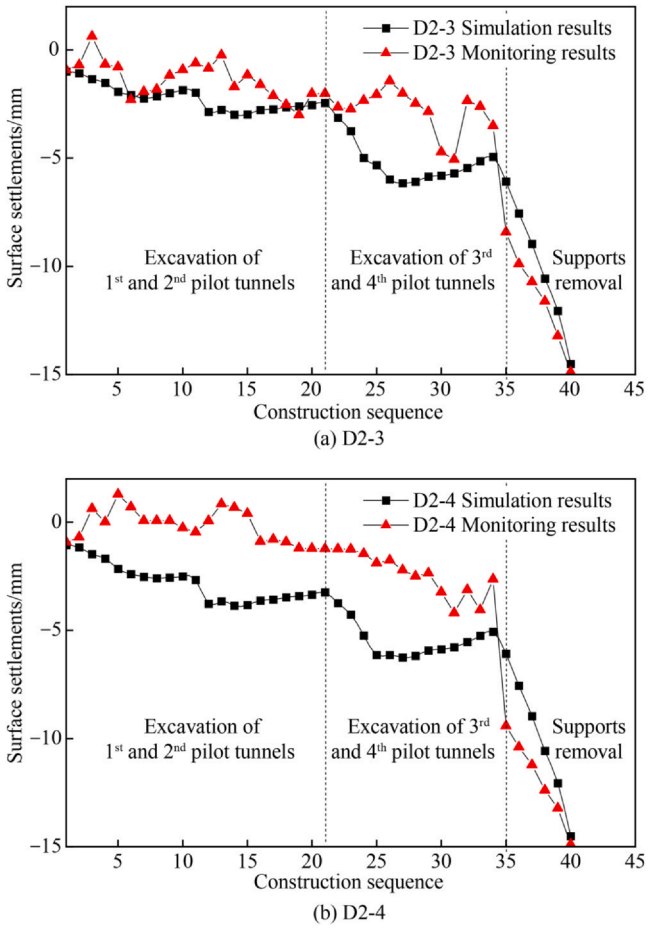

Fig. 10. Comparison of numerical simulation results for surface settlements and monitoring data.

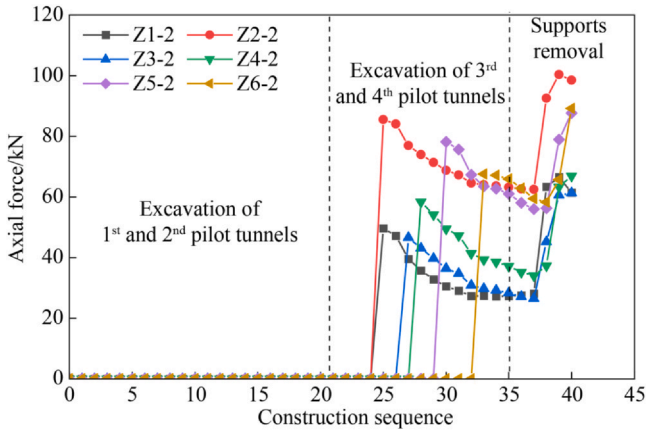

Fig. 11. Axial force of tie rods in the second row at different construction stages.

4.3. Axial force of tie rods

Fig. 11 shows the axial force of tie rods in the second row at different construction stages. The following conclusions can be drawn:

1) During the excavation process, a consistent trend in axial force changes was observed in the two rows of tie rods positioned above the 1st pilot (ZCL1-4 to ZCL6-4 and ZCL1-3 to ZCL6-3) displayed a consistent trend in axial force changes, featuring both increasing and decreasing sections. Throughout the whole excavation process, the maximum axial force recorded in the two rows of tie rods above the 1st pilot reaches 110 kN, while the minimum axial force registers at − 4.24 kN, which remains below the maximum allowable value.
2) During the excavation process, the axial force changes displayed a similar pattern when considering the two rows of tie rods above the 3rd pilot (ZCL1-1 to ZCL6-1 and ZCL1-2 to ZCL6-2). There is minimal fluctuation in the axial force during the excavation of the first two pilot tunnels, as these two rows of tie rods are not connected to the lining structure. Any slight changes are likely due to the friction

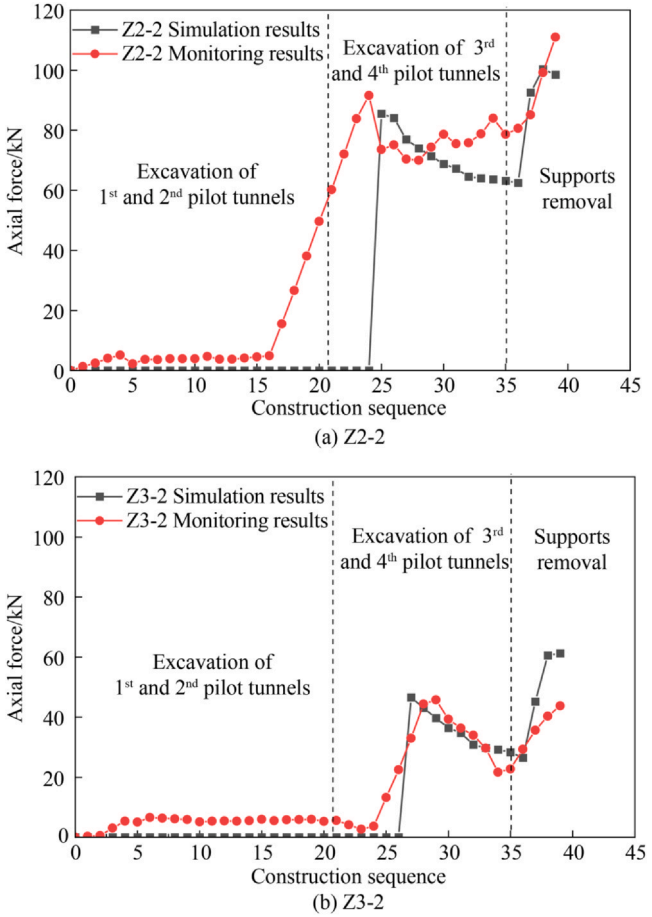

Fig. 12. The comparison between the simulated axial forces at monitoring points and the on-site monitoring measurements.

between the tie rods and the sleeve. Conversely, when excavating the No. 3 and No. 4 guide holes, the axial force in both rows of tie rods increases almost simultaneously. This phenomenon results from the larger excavation footage of the No. 3 and No. 4 guide holes.

3) During the demolition of the central diagram and the installation of the secondary lining, the axial force values for the two rows of tie rods situated above the 1st pilot showed an upward trend. The maximum axial force recorded was 165.03 kN, while the minimum axial force was − 37.17 kN, both of which were below the maximum allowable threshold.
4) The axial force values of the two rows of tie rods located above the 3rd pilot varied during the demolition of the central partition wall and the installation of the secondary lining, with both upward and downward trends observed. The maximum axial force measured was 228.07 kN, and the minimum axial force was − 41.91 kN, both of which were within the permissible limits.
5) The axial force variations of the second-row tie rods with respect to construction steps are depicted in Fig. 11. During the excavation of tunnels 1 and 2 (construction steps 1–21), the tie rods in the third row, positioned above tunnels 3 and 4, remained unconnected to the initial support, resulting in an axial force of 0. As the excavation proceeded for tunnels 3 and 4 (construction steps 22–34), the axial force in the tie rods gradually increased as the excavation reached the location of the tie rods, reaching a maximum of 86.02 kN. Subsequently, as the excavation continued into the surrounding soil, the axial force in the tie rods began to decrease. After the removal of the central partition (construction steps 35–39), the loss of support from the partition led to the release of stress within the surrounding soil. This stress was subsequently borne by the tie rods, resulting in another increase in axial force, reaching a maximum of 100.88 kN.

Fig. 12 illustrates the comparison between the numerical simulation values and the on-site monitoring measurements for tie rod axial forces at the monitoring points. It is evident that both monitoring points exhibit a pattern of increase, decrease, and subsequent increase in tie rod axial forces. Upon completion of construction, values from numerical simulation and on-site monitoring of axial forces for monitoring point Z2-2 showed 98.49 and 110.99 kN, respectively. Similarly, the numerical simulation value for monitoring point Z3-2 was 61.25 kN, in comparison to the on-site monitoring point Z3-2 was 43.63 kN. Overall, the trends in axial force values for tie rods in construction were in accordance with the numerical simulation and field monitoring data.

During the initial construction process, tie rods experience minimal axial forces in the numerical simulation until they are attached to the initial support. However, in engineering practice, tie rods start to bear loads as soon as they are embedded in the ground, resulting in initial low axial force values. During the initial phase of the first upward trend in axial force for tie rods, monitoring data exhibit a more gradual change than the simulation results. The primary distinction between simulations and real-life construction processes is that the stress caused by soil excavation in simulations is completely alleviated once the construction is complete, whereas, stress release is a gradual process.

5. Conclusions

A novel tunnel excavation construction method, the suspension method, is proposed. The proposed method can be effectively utilized in both railway and subway tunnels to satisfy the requirements of settlement control. This method is employed in a trial block of Harbin Metro Line 3 for practical applications. The performance of the suspension method was then elaborated and analyzed through a combination of numerical simulations and on-site monitoring measurements. The conclusions are summarized as follows:

1) The proposed method employs vertical tie rods to establish a structural connection between the initial tunnel support system and the surface steel beam, thereby providing effective control of settlements.
2) Numerical simulations were conducted to analyze ground surface settlement and vault settlement during tunnel excavation. The surface settlement troughs induced by tunneling were generally symmetric with respect to the tunnel centerline and the maximum surface settlement value of a section was reported above the tunnel centerline. The results showed that the suspension method is superior to the traditional CRD method and double-side drift method in terms of controlling settlement, with the maximum ground surface settlement induced by excavation being 14.51 mm.
3) The axial force of the tie rod is affected by the analysis. The axial force of the tie rod is affected by the excavation stages, with the maximum axial force occurring when all supports are removed. Throughout the construction process, all tie rod axial forces remain in compliance with the design requirements.
4) The on-site monitoring results are in agreement with the numerical simulation analysis, thus affirming the effectiveness of the proposed method. Additionally, remarkable settlement fluctuations occur during the winter break, mainly caused by the freezing of the soil in winter and its thawing in spring. Consequently, the importance of on-site monitoring during winter break cannot be overlooked, as the impact of soil freezing and thawing should not be underestimated.

Conflict of interest

The authors declare that they have no competing interests.

Acknowledgment

This work was supported by the Fundamental Research Funds for the Central Universities (2023JBZD004) , the National Natural Science

Foundation of China (U2034204, 52078031), and the Science and Technology Development Project of CCCC Harbin Metro Investment and Construction Co., Ltd. (ZJHD-FW-2018–01-086).

References

[1] Y. Yuan, X. Jiang, X. Liu, Predictive maintenance of shield tunnels, Tunnel. Undergr. Space Technol. 38 (2013) 69–86.
[2] T.E. Vorster, A. Klar, K. Soga, et al., Estimating the effects of tunneling on existing pipelines, J. Geotech. Geoenviron. Eng. 131 (11) (2005) 1399–1410.
[3] S.M. Liao, J.H. Liu, R.L. Wang, et al., Shield tunneling and environment protection in Shanghai soft ground, Tunnel. Undergr. Space Technol. 24 (4) (2009) 454–465.
[4] Z. Zhang, M. Huang, Geotechnical influence on existing subway tunnels induced by multiline tunneling in Shanghai soft soil, Comput. Geotech. 56 (2014) 121–132.
[5] X. Liu, Y. Liu, Z. Yang, et al., Numerical analysis on the mechanical performance of supporting structures and ground settlement characteristics in construction process of subway station built by Pile-Beam-Arch method, KSCE J. Civ. Eng. 21 (5) (2017) 1690–1705.
[6] V. Romero, NATM in soft ground: a contradiction in terms? World Tunn. 15 (7) (2002) 338–340.
[7] M. Lei, L. Peng, C. Shi, Model test to investigate the failure mechanisms and lining stress characteristics of shallow buried tunnels under unsymmetrical loading, Tunnel. Undergr. Space Technol. 46 (2015) 64–75.
[8] D. Zhang, Q. Fang, P. Li, et al., Structural responses of secondary lining of high-speed railway tunnel excavated in loess ground, Adv. Struct. Eng. 16 (8) (2013) 1371–1379.
[9] F. Tonon, ADECO full-face tunnel excavation of two 260 m^2 tubes in clays with sub-horizontal jet-grouting under minimal urban cover, Tunnel. Undergr. Space Technol. 26 (2) (2011) 253–266.
[10] M. Karakus, R. Fowell, 2-D and 3-D finite element analyses for the settlement due to soft ground tunneling, Tunnel. Undergr. Space Technol. 21 (3) (2006).
[11] Q. Fang, D.L. Zhang, L.N.Y. Wong, Shallow tunneling method (STM) for subway station construction in soft ground, Tunnel. Undergr. Space Technol. 29 (2012) 10–30.
[12] M. Sharifzadeh, F. Kolivand, M. Ghorbani, et al., Design of sequential excavation method for large span urban tunnels in soft ground-Niayesh tunnel, Tunnel. Undergr. Space Technol. 35 (2013) 178–188.
[13] C. Yoo, Performance of multi-faced tunneling—a 3D numerical investigation, Tunnel. Undergr. Space Technol. 24 (5) (2009) 562–573.
[14] F.C. Xue, J.L. Ma, L. Yan, et al., Three-dimension FEM analysis of large cross-section tunnel in collapsible loess constructed by CRD method, : GeoFlorida 2010: Adv. Anal., Model. Des. (2010) 2349–2358.
[15] Q. Fang, X. Liu, D. Zhang, et al., Shallow tunnel construction with irregular surface topography using cross diaphragm method, Tunnel. Undergr. Space Technol, (2017), pp. 11–21.
[16] P. Li, Y. Zhao, X. Zhou, Displacement characteristics of high-speed railway tunnel construction in loess ground by using multi-step excavation method, Tunnel. Undergr. Space Technol. 51 (2016) 41–55.
[17] J. Lai, J. Qiu, H. Fan, et al., Fiber bragg grating sensors-based in situ monitoring and safety assessment of loess tunnel, J. Sens 16 (2016) 1–10.
[18] J. Zhang, M. Wang, S. Yu, Analysis on deformation of central diaphragms of tunnels constructed by CRD method: case study on Xiang'an sub-sea tunnel in Xiamen, China Tunn. Constr. 27 (4) (2007) 16–19.